Journal of Power Sources 196 (2011) 5823–5828

Contents lists available at ScienceDirect

Journal of Power Sources

journal homepage: www.elsevier.com/locate/jpowsour

Novel nanocrystalline PdNi alloy catalyst for methanol and ethanol electro-oxidation in alkaline media

Zhen Qi[a], Haoran Geng[b], Xiaoguang Wang[a], Changchun Zhao[a], Hong Ji[a], Chi Zhang[a], Junling Xu[a], Zhonghua Zhang[a,*]

[a] Key Laboratory for Liquid–Solid Structural Evolution and Processing of Materials (MOE), School of Materials Science and Engineering, Shandong University, Jingshi Road 17923, Jinan 250061, PR China
[b] School of Materials Science and Engineering, University of Jinan, Jiwei Road 106, Jinan 250022, PR China

ARTICLE INFO

Article history:
Received 26 January 2011
Accepted 28 February 2011
Available online 5 March 2011

Keywords:
Direct alcohol fuel cells
Electro-oxidation
Alloy catalyst
Dealloying
Nanoporous alloys

ABSTRACT

Nanocrystalline $Pd_{40}Ni_{60}$ alloy catalyst has been fabricated by dealloying a ternary $Al_{75}Pd_{10}Ni_{15}$ alloy in a 20 wt.% NaOH aqueous solution under free corrosion conditions. The microstructure and catalytic performance of the catalyst have been characterized by X-ray diffraction, scanning electron microscopy, transmission electron microscopy, high-resolution transmission electron microscopy, and cyclic voltammetry. The $Pd_{40}Ni_{60}$ alloy consists of nanocrystals with sizes of 5–10 nm, and Pd/Ni elements exist in a solid solution form. Moreover, nanocrystalline zones, amorphous zones and lattice distortion can be observed in the $Pd_{40}Ni_{60}$ alloy. Electrochemical measurements demonstrate that, for equivalent mass Pd, $Pd_{40}Ni_{60}$ has an enhanced electrocatalytic performance towards methanol and ethanol oxidation in alkaline media than nanoporous Pd. The nanocrystalline $Pd_{40}Ni_{60}$ alloy is a promising catalyst towards alcohol oxidation in alkaline media for fuel cell applications.

1. Introduction

In recent years, great attention has been paid to direct alcohol fuel cells (DAFCs) as portable applications due to some superior advantages over analogous devices fed with hydrogen [1]. The most common DAFC is the *direct methanol fuel cell* (DMFC). Up to date, most of researches on DMFC have been done in acidic media with Pt and Pt-based alloys as anode catalysts due to their high catalytic ability in various reactions including electro-oxidation of small organic molecules [2–4]. However, Pt-based catalysts suffer some disadvantages, such as CO poisoning, effective methanol crossover, degradation of membranes, and corrosion of carbon materials and cell hardware [5]. In comparison, if DMFCs operate in an alkaline electrolyte, the kinetics would be significantly improved and Pt-free electrocatalysts could be used [6].

Pd, which is one of platinum group elements, holds high electro-oxidation catalytic activity and has larger abundance and lower price compared to Pt [7,8]. The interest in Pd is not only for the purpose to lower the cost of catalysts but pursuits an improved catalytic activity. One method to promote the catalytic activity of Pt is alloying with another metal, such as Ru, Sn, etc. [9–11]. Similarly, the catalytic activity of Pd can be modified by alloying with other metals, among which Ni is the main focus. Liu et al. [12] synthesized PdNi nanoparticles by a chemical reduction process with formic acid. Both electrodeposited bimetallic PdNi film [13] and PdNi alloy [14] show an enhanced catalytic activity than pure Pd synthesized with the same processes. In addition, the combination of Pd with Ni is expected to further enhance the tolerance of Pd to poisoning as Ni is an oxophilic element.

In our previous work, we have successfully fabricated nanoporous Pd (NPPd) by dealloying an Al–Pd alloy and have found that NPPd has an ultrahigh electrochemical active surface area and exhibits a superior catalytic performance with high stability [15]. With the inspiration of Pt or Pd alloyed with another metal to improve the catalytic activity, we aim to investigate a nanocrystalline PdNi alloy fabricated by dealloying a ternary AlPdNi precursor. The catalytic activity of the fabricated PdNi alloy for methanol and ethanol electro-oxidation has also been studied.

2. Experimental

The starting $Al_{75}Pd_{10}Ni_{15}$ (nominal composition, at.%) ribbons were prepared by a melt spinning technique from pure Al (99.95 wt.%), Pd (99.9 wt.%) and Ni (99.9 wt.%) ingots at a rotation speed of 1000 rpm in a controlled Ar atmosphere on a copper roller with a diameter of 0.35 m. The ribbons obtained were typically 20–50 μm in thickness, 2–4 mm in width, and several centimeters in length. The dealloying was performed in a 20 wt.% NaOH aqueous

* Corresponding author. Tel.: +86 531 88396978; fax: +86 531 88395011.
E-mail address: zh_zhang@sdu.edu.cn (Z. Zhang).

0378-7753/$ – see front matter © 2011 Elsevier B.V. All rights reserved.
doi:10.1016/j.jpowsour.2011.02.083

solution (prepared from analytical grade reagents and nanopure water) first at room temperature for 1 h and then at 90 ± 5 °C for another 1 h until no obvious bubbles emerged. Finally, the samples were rinsed in distilled water for several times to remove the residual NaOH.

The microstructure of the melt-spun $Al_{75}Pd_{10}Ni_{15}$ precursor and the as-dealloyed samples was characterized by X-ray diffraction (XRD, Rigaku D/max-rB) with Cu Kα radiation, a scanning electron microscope (SEM, LEO 1530VP) with an energy dispersive X-ray analyzer (EDX), a transmission electron microscopy (TEM, Philips CM 20) with selected-area electron diffraction (SAED) and a high-resolution TEM (HRTEM, FEI Tecnai G2). TEM specimens were prepared using a Gatan ion mill at 5 kV. The fast Fourier transform (FFT) patterns were obtained from the corresponding HRTEM images using a Gatan software.

All electrochemical measurements were performed in a standard three-electrode cell using a LK 2005A Potentiostat. The electro-oxidation electrode was prepared as follows: 4 mg fine ground as-dealloyed samples, 4 mg Vulcan XC-72 carbon powders, 300 μL isopropanol, and 100 μL Nafion solution (0.5 wt.%) were ultrasonically mixed for 30 min. Then, 5 μL of the homogeneously mixed ink was placed on a freshly polished glassy carbon (GC) electrode with a diameter of 4 mm. The counter electrode was a bright Pt plate, a saturated calomel electrode (SCE) or Hg/HgO electrode (MMO) was used as the reference electrode, depending upon the experimental requirement. Cyclic voltammetric (CV) tests were performed in the potential range of −1.0 to 1.0 V (vs. MMO) in a solution of 1.0 M KOH, and −0.9 to 0.6 V (vs. MMO) in solutions of 1.0 M KOH + 0.5 M methanol or 1.0 M KOH + 1.0 M ethanol at a scan rate of 50 mV s^{-1}. For comparison, CV tests of the catalyst electrode were also carried out in the potential range of −0.25 to 1.1 V (vs. SCE) in the 1.0 M H_2SO_4 solution, and then electrocatalytic activities were measured in the solutions of 1.0 M KOH + 0.5 M methanol and 1.0 M KOH + 1.0 M ethanol at a scan rate of 50 mV s^{-1}. All electrochemical experiments were performed at ambient temperature (~25 °C). All current densities were calculated according to geometric areas of electrodes and were normalized to equivalent mass Pd. NPPd was also prepared for comparison to evaluate the electrocatalytic performance of the as-dealloyed alloy catalyst [15].

3. Results and discussion

Fig. 1a shows the XRD pattern of the melt-spun $Al_{75}Pd_{10}Ni_{15}$ alloy. Al, Al_3Ni, Al_3Pd and other unknown phases (unlabelled peaks which cannot be indexed to any known phase) exist in the starting precursor alloy. It is known that the Al–TMs (transition metals) systems are easy to form metastable phases, especially under rapid solidification conditions. Fig. 1b shows the XRD pattern of the as-dealloyed samples obtained via dealloying of $Al_{75}Pd_{10}Ni_{15}$ in the 20 wt.% NaOH solution. The peaks at 41.3, 48.3 and 70.9° can be assigned to (1 1 1), (2 0 0) and (2 2 0) reflections of an fcc PdNi solid solution, and no Pd or Ni peaks can be found in this XRD profile. Thus, the Al, Al_3Ni, Al_3Pd and other unknown phases in the precursor can be fully dealloyed in the NaOH solution. In addition, a little amount of NiO exists in the as-dealloyed samples. Line broadening is obvious, which indicates grain refinement in the as-dealloyed samples. According to the X-ray profile broadening, the mean crystallite size of the as-dealloyed samples can be evaluated using the classical Scherrer equation [16]:

$$\beta_{hkl} = \frac{K\lambda}{T\cos\theta_{hkl}}$$

where β_{hkl} is the crystallite size contribution to the peak width (integral or full width at half maximum) in radians, K is a constant near unity (here, 0.9 was used), λ is the wavelength of X-ray (here, 0.15406 nm), θ_{hkl} is the peak position of the reflection (hkl), and T is the average thickness of the crystal in a direction normal to the diffracting plane (hkl). In the present work, the PdNi (1 1 1) reflection was used and the mean size was calculated to be ~2 nm.

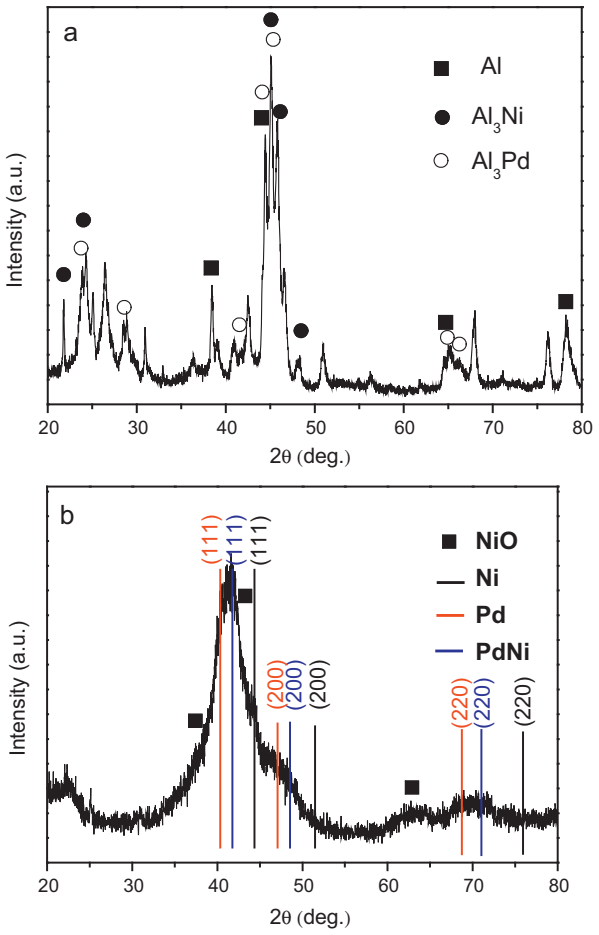

Fig. 1. XRD patterns of the melt-spun $Al_{75}Pd_{10}Ni_{15}$ alloy before (a) and after (b) dealloying in the 20 wt.% NaOH solution.

Fig. 2 shows the SEM images of the cross-sectioned view of the as-dealloyed samples. Two distinguished areas can be observed in the as-dealloyed samples. According to solidification sequence of the ribbon, one is the columnar area which grows along the vertical direction (highlighted by a downward arrow in Fig. 2a) due to the direct contact of liquid melt with the copper roller during the rapid solidification process. The other is the equiaxed area which is not in contact with the copper roller (highlighted by an upward arrow in Fig. 2a) and thus solidifies later than the columnar area. The as-dealloyed samples consist of short rods with several microns in length and hundreds of nanometers in diameter (Fig. 2b). Moreover, the rods form clusters in local areas, and one cluster is highlighted by an arrow in Fig. 2b. Within the cluster, all rods are approximately parallel. No obvious nanopores are found in the as-dealloyed samples from SEM at a higher magnification (Fig. 2c). Only large channels among short rods can be observed, as marked by arrows in Fig. 2c. In comparison, a typical nanoporous structure with ligament/channel sizes of 3–6 nm can be observed in NPPd obtained via alkaline dealloying [15]. In addition, NPPd obtained via acid dealloying [17] also shows a similar rod-like morphology with the same size, however, small pores with a size of 15–20 nm can be clearly observed from the SEM images. We have attributed the formation of this microstructure to two processes: on one hand, the Al is more prone to be attacked by corrosive solutions than the Al_3Pd allowing the formation of large channels to form; on the other

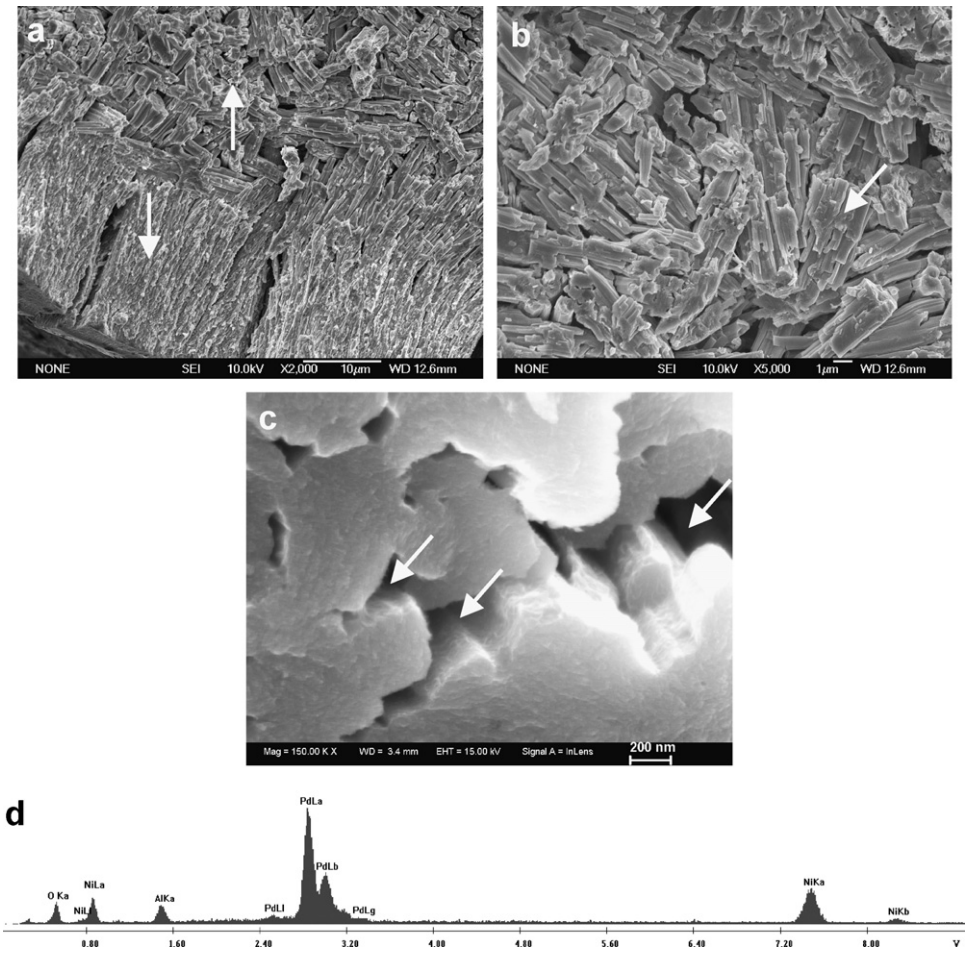

Fig. 2. SEM images (a, b and c) showing the cross-sectioned view of the as-dealloyed sample. (d) A typical EDX spectrum showing the composition of the as-dealloyed sample.

hand, the removal of Al from Al_3Pd results in the formation of small nanopores while the columnar structure formed in the precursor is kept during the dealloying process. When the large channels form, the corrosive solution can penetrate into these channels where once the Al surrounds the unattacked phases and dealloying continually executes on the unattacked phases. It is obvious that the formation of the present PdNi alloy can be explained by the above mechanism. However, no nanopores can be observed in the present PdNi alloy. It should be noted that nanoporous Au, Ag and Cu can be obtained from Al–Au, Al–Ag and Al–Cu alloys with the same alkaline solution under similar dealloying conditions [18–20]. In our previous study of porous Ni [21] prepared with same method, the morphologies of porous Ni inherit from those of the precursor alloys. However, no nanopores were found in porous Ni samples. Therefore, the morphologies of grains in the precursor alloys can be inherited into the as-dealloyed samples during the dealloying process. It is generally deemed that the formation of a nanoporous structure through dealloying is via the surface diffusion of more noble metals. When Al is removed from the Al_3Ni, Al_3Pd and other unknown phases, Ni and Pd in those phases form adatoms at the metal/solution interface. Then, those adatoms diffuse and aggregate to form the present microstructure. Unlike the single diffusion of only one metal (for example, Pd, Au, Ag, Cu and Ni), however, the surface diffusion of two metals is highly influenced by their different diffusivities. As for the present case, Ni plays a dominant role in the formation of the present microstructure of the as-dealloyed samples, due to the fact that nanopores can be obtained for NPPd and nanoporous Au, Ag and Cu, while no nanopores exist in porous Ni. Furthermore, there has been no report of successful synthesis of nanoporous Ni from Al–Ni alloys. There are indeed some reports that nanoporous Ni has been fabricated from Ni–Cu and Mn–Ni alloys [22,23]. The reason why Al–Ni cannot be used to obtain nanoporous Ni is still unclear, and it needs further study which is not the focus of this work. Fig. 2d shows a typical EDX spectrum of the as-dealloyed samples. It can be found that there is some residual Al existing but the amount of Al is only several atom percent. The Pd/Ni atomic ratio is close to 2:3 (37:63) in the as-dealloyed samples, and thus the as-dealloyed alloy was designated as $Pd_{40}Ni_{60}$ for simplicity. In addition, O element can be found in the EDX spectrum which can be recognized as NiO according to the XRD result. NiO has also been found in porous Ni obtained from Al–Ni alloys via dealloying [21].

Fig. 3 shows the TEM image of the as-obtained $Pd_{40}Ni_{60}$ alloy. Although the image contrast is inhomogeneous, it is clear that neither nanopores nor ligaments can be observed in the microstructure of the $Pd_{40}Ni_{60}$ alloy. The corresponding SAED pattern consists of diffraction rings, demonstrating that the $Pd_{40}Ni_{60}$ alloy is composed of nanocrystals (inset of Fig. 3). The HRTEM image shows that these nanocrystals are 5–10 nm in size (one nanocrystal is marked by a dashed ellipse in Fig. 4). The size of these nanocrystals is a little larger than that determined by the Scherrer law according to the XRD result (Fig. 1b). Besides nanocrystals, some amorphous zones and lattice distortion can be observed as highlighted by a dashed square and a solid ellipse in Fig. 4, respectively. The formation of these unique structures may be attributed to the employment of dealloying to fabricate the nanocrystalline $Pd_{40}Ni_{60}$ alloy. In addition, the corresponding FFT pattern further verifies the nanocrystalline nature of the $Pd_{40}Ni_{60}$ alloy (inset of Fig. 4).

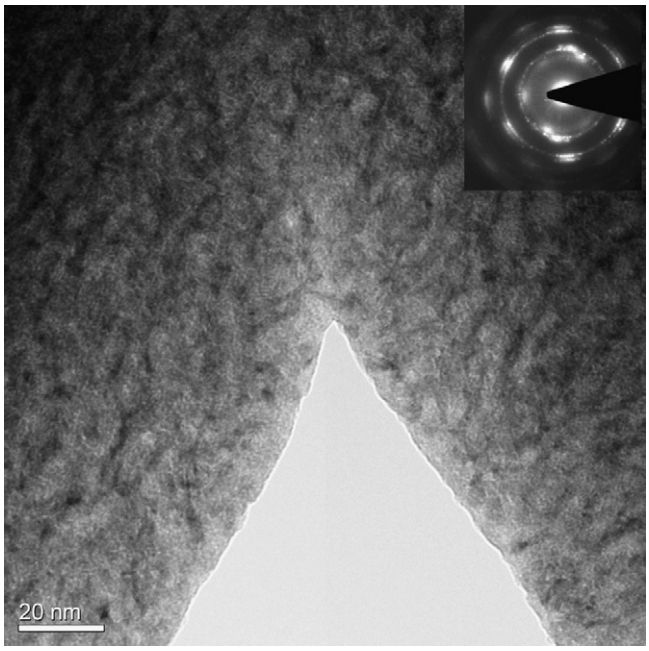

Fig. 3. TEM image of the nanocrystalline $Pd_{40}Ni_{60}$ alloy and corresponding SAED pattern (inset).

Fig. 5a shows CV curves of $Pd_{40}Ni_{60}$ and NPPd in the 1.0 M KOH solution. It can be seen that the desorption/adsorption of hydrogen appearing between −1.0 and −0.74 V is clearly shown for NPPd. In comparison, the desorption/adsorption peaks appear between −1.0 and −0.43 V for $Pd_{40}Ni_{60}$, which are more distinguishable than those of NPPd. As shown in Fig. 5a, the current peaks associated with the reduction of Pd (II) species, either PdO or $Pd(OH)_2$, are located at −0.46 and −0.37 V in the back scan for $Pd_{40}Ni_{60}$ and NPPd, respectively. Additionally, a pair of redox peaks (A and A') are detected on the CV curve of $Pd_{40}Ni_{60}$ which can be attributed to the interconversion of $Ni(OH)_2$ and NiOOH in alkaline media [24]. The good symmetry of the redox peaks indicates reversibility of this

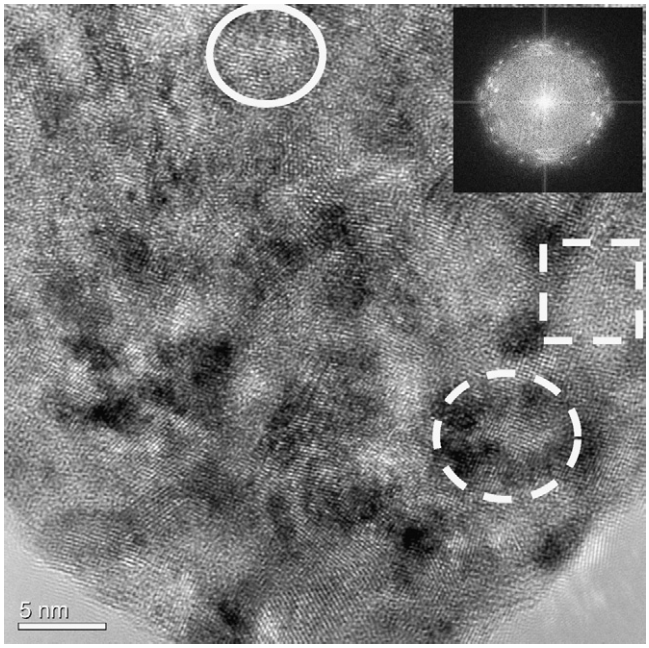

Fig. 4. HRTEM image of the nanocrystalline $Pd_{40}Ni_{60}$ alloy and corresponding FFT pattern (inset).

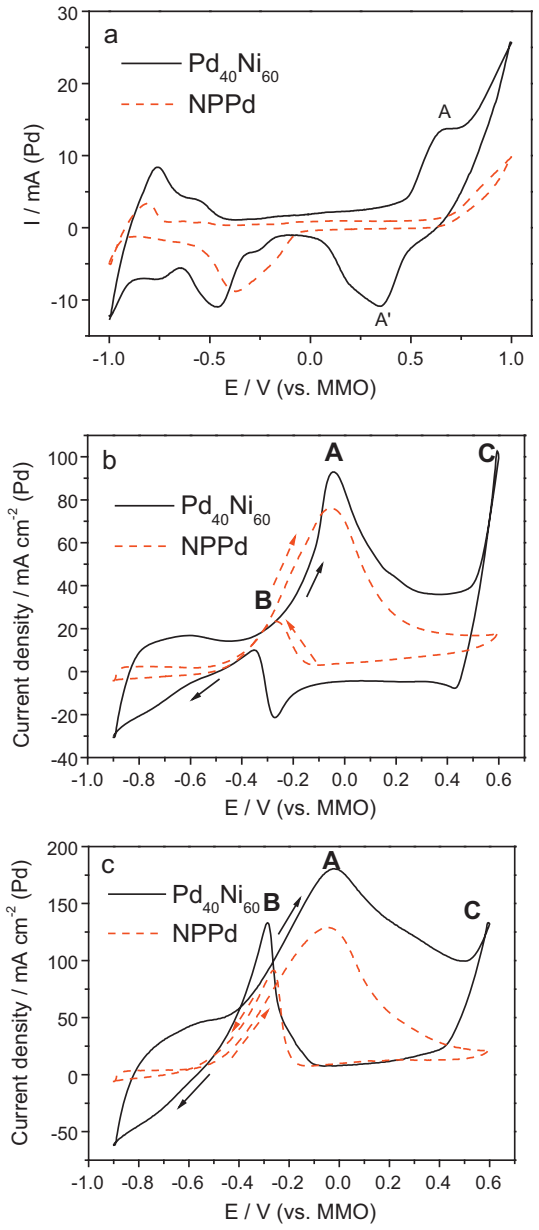

Fig. 5. CV curves of the $Pd_{40}Ni_{60}$ and NPPd catalysts in the solutions of 1.0 M KOH (a), 1.0 M KOH + 0.5 M methanol (b) and 1.0 M KOH + 1.0 M ethanol (c).

reaction. The voltammograms of NPPd and $Pd_{40}Ni_{60}$ are similar to the reported results of Pd and PdNi alloy [12].

Fig. 5b shows CV curves of $Pd_{40}Ni_{60}$ and NPPd for methanol electro-oxidation in the solution of 1.0 M KOH + 0.5 M methanol. In the forward scan, the onset potential of $Pd_{40}Ni_{60}$ is −0.83 V, which negatively shifts by ~300 mV as compared to that of NPPd (−0.53 V). This means that the overpotential in methanol oxidation can be significantly reduced by the nanocrystalline $Pd_{40}Ni_{60}$ alloy [25,26]. The peak current densities are 93 and 76 mA cm^{-2} for $Pd_{40}Ni_{60}$ and NPPd, respectively, while their peak potentials are comparable. In addition, the ratio of the forward anodic peak current (I_f) to the backward anodic peak current (I_b), I_f/I_b, may be used to evaluate the tolerance of catalysts to accumulation of carbonaceous species. A higher ratio indicates more effective removal of poisoning species on the catalyst surface. The I_f/I_b ratio of $Pd_{40}Ni_{60}$ is ~9.3, which is nearly three times that of NPPd (3.3). The present result of the methanol oxidation reaction is consistent with Pd-MWCNT-Ni composites [6]. Two well defined anodic current peaks

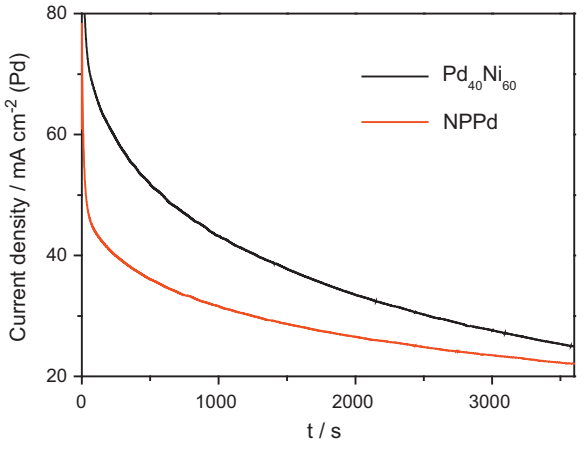

Fig. 6. Chronoamperometric curves of the $Pd_{40}Ni_{60}$ and NPPd catalysts in the solution of 1.0 M KOH + 1.0 M ethanol at a fixed potential of −100 mV for 3600 s.

can be characterized: one in the forward (A) (i.e., under anodic condition) and the other one (B) in the backward (i.e., under cathodic condition) scan (Fig. 5b). The oxidation current peak A is correlated with the oxidation of freshly chemisorbed species coming from methanol adsorption [27,28]. The origin of oxidation peak B is still under debate. Some researchers have suggested that the current peak in the backward scan is primarily associated with removal of carbonaceous species not completely oxidized in the forward scan, rather than caused by freshly chemisorbed species [6,29–31]. While others have argued that the current peak in the backward scan cannot be ascribed to the removal of intermediate species but be related to the oxidation of the methanol molecules in the electrolyte [32–34]. Still much more work should be done to help understand the origin of the current peak in the backward scan. Peak C is owing to the oxidation process of $Ni(OH)_2$ to NiOOH [13].

Fig. 5c shows CV curves of $Pd_{40}Ni_{60}$ and NPPd for ethanol electro-oxidation in the solution of 1.0 M KOH + 1.0 M ethanol. The onset potential of $Pd_{40}Ni_{60}$ (−0.81 V) negatively shifts by ~240 mV as compared to that of NPPd (−0.57 V). Furthermore, the peak current densities are 180 and 129 mA cm^{-2} for $Pd_{40}Ni_{60}$ and NPPd, respectively. Recently, Liang et al. [34] have proposed a mechanism for ethanol oxidation reaction on palladium in alkaline media:

$$Pd + CH_3CH_2OH \leftrightarrow Pd\text{–}(CH_3CH_2OH)_{ads} \quad (1)$$

$$Pd\text{–}(CH_3CH_2OH)_{ads} + 3OH^- \rightarrow Pd\text{–}(CH_3CO)_{ads} + 3H_2O + 3e^- \quad (2)$$

$$Pd\text{–}(CH_3CO)_{ads} + Pd\text{–}OH_{ads} \rightarrow Pd\text{–}CH_3COOH + Pd \quad (3)$$

$$Pd\text{–}CH_3COOH + OH^- \rightarrow Pd + CH_3COO^- + H_2O : \text{fast} \quad (4)$$

The change of CVs in desorption/adsorption of hydrogen region can be attributed to the dissociative adsorption of ethanol by Eqs. (1) and (2). The resultant ethoxi, such as $(CH_3CO)_{ads}$, is strongly adsorbed onto the active sites of the Pd electrode, which blocks the ab/adsorption of hydrogen, thereby reducing the hydrogen peaks. The adsorbed intermediates formed during the dissociative adsorption of ethanol can be stripped off the Pd electrode by the adsorbed oxygen-containing species ($Pd\text{–}OH_{ads}$). As a result, the ethanol oxidation reaction can proceed continuously such that the current continues to increase with the potential, which leads to the formation of peak A. Peaks B and C are the same as the case of methanol oxidation reaction in alkaline solutions. In order to evaluate the stability of the $Pd_{40}Ni_{60}$ alloy versus NPPd, chronoamperometry was employed and the results are shown in Fig. 6. The present results show that the current densities represent less decay at the applied constant potentials for a long duration (3600 s), indicating that the nanocrystalline $Pd_{40}Ni_{60}$ alloy exhibits a better stable

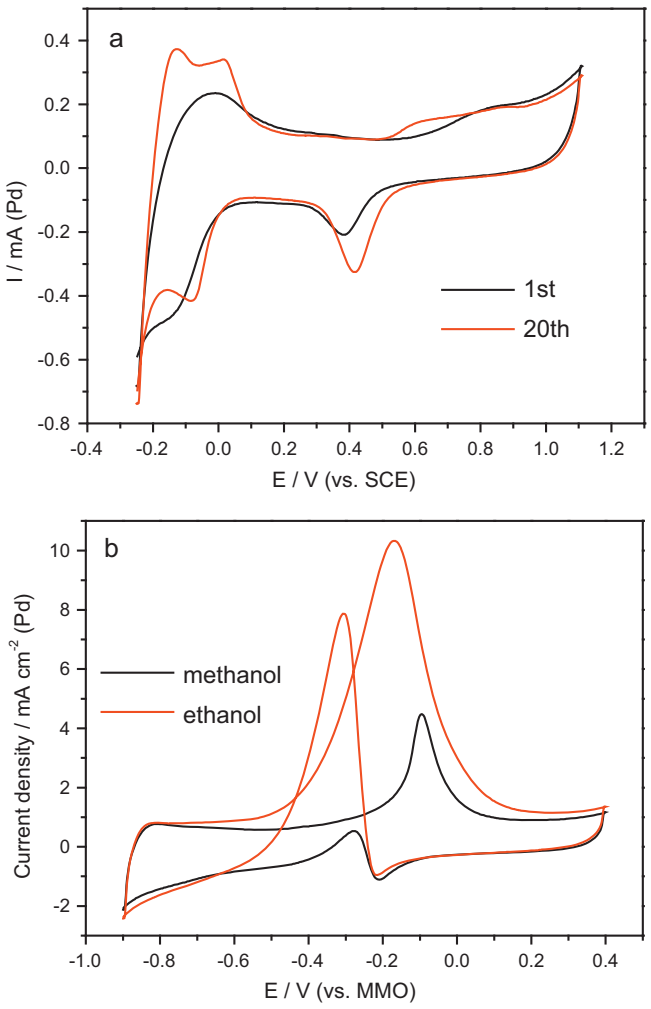

Fig. 7. CV curves of the $Pd_{40}Ni_{60}$ catalyst (1st and 20th cycles) scanned in the 1.0 M H_2SO_4 solution (a) and then in the solutions of 1.0 M KOH + 0.5 M methanol and 1.0 M KOH + 1.0 M ethanol (b).

electrocatalytic activity towards ethanol oxidation in the alkaline media than NPPd. It is generally believed that lower onset potential and higher peak current are key parameters to evaluate the catalytic performance of a catalyst. Therefore, the nanocrystalline $Pd_{40}Ni_{60}$ alloy has a better catalytic activity than NPPd for alcohol electro-oxidation in alkaline solutions.

In the study of NPPd, the electrode was scanned in a sulfuric acid solution. We also conducted this experiment and the results are shown in Fig. 7a. It can be seen that the CV curve of the 1st cycle is different from that of the 20th cycle. Moreover, the potential of reduction peak in the back scan positively shifts with increasing cycles. The CV profile of the $Pd_{40}Ni_{60}$ alloy after 20 cycles is similar to that of NPPd when scanned in the acid solution [15]. In a study on the effect of Ni addition over PtRu/C based electrocatalyst [35], they have found that the CV of Pt–Ni sample after 100 cycles is similar to that of Pt in the H_2SO_4 solution. Using X-ray photoelectron spectra (XPS) and inductively coupled plasma (ICP) analysis, they have found that neither Ni nor Pt can be detected in the scanned solution, and have believed that the migration of the Ni to the inner layers of the solids results in the surface enrichment of Pt during the electrochemical measurement [35]. Therefore, the CV evolution in the present work may be associated with the migration of Ni from the surface to the inner part of the $Pd_{40}Ni_{60}$ catalyst (Fig. 7a). The $Pd_{40}Ni_{60}$ catalyst scanned in the acid solution was tested in the alkaline solution with alcohols to characterize its

catalytic performance. Fig. 7b shows CV curves of the $Pd_{40}Ni_{60}$ catalyst in the solutions of 1.0 M KOH + 0.5 M methanol and 1.0 M KOH + 1.0 M ethanol. It can be found that the catalytic performance of $Pd_{40}Ni_{60}$ is not enhanced. This indicates that the enhanced performance of the $Pd_{40}Ni_{60}$ alloy is highly related to the Ni addition.

In comparison with NPPd, in which the superior electrocatalytic activity is attributed to the enhanced amount of active sites resulting from the unique bicontinuous ultrafine nanoporous structure (see Ref. [15]), the microstructure of $Pd_{40}Ni_{60}$ shows no nanopore inside as shown in Figs. 2–4. However, the unique microstructure (nanocrystalline zones, amorphous zones and lattice distortion) of $Pd_{40}Ni_{60}$ may also provide comparable active sites as NPPd. The enhanced electro-oxidation performance of $Pd_{40}Ni_{60}$ can be ascribed to alloying effect of Ni. Alloying is an effective way of changing the reactivity of a given metal [36]. If so, the bond strength of the adsorbed species and thereby their reactivity may change as well. It can have different effects: (i) increase in possible geometries of adsorbates and reaction complexes; (ii) change in electronic structures of the alloy in comparison to those of pure constituent elements; (iii) surface segregation of one element. The electronic state of Pd is modified by alloying with Ni, which promotes the catalytic activity of Pd towards methanol and ethanol electro-oxidation. This is verified by the XRD result which shows that Pd and Ni are well alloyed. The Pd d-band centre shifts down when Pd is alloyed with Ni, similar to PtRu. This suggests weaker Pd-adsorbate bonding, while the Ni d-band centre slightly shifts up. In other words, when Pd and Ni are alloyed, the adsorption of adsorbates is weaker on the Pd sites and stronger on the Ni sites. Therefore, the poisoning species are prone to adsorb on Ni rather than Pd. This is supported by the high ratio of I_f/I_b of the $Pd_{40}Ni_{60}$ alloy, indicating a better poisoning tolerance towards methanol oxidation reactions. In addition, the transfer of electrons from Ni to Pd may occur since the electronegativity of Ni is 1.91 while that of Pd is 2.20 [6]. This can decrease the Pd–CO binding energy, improve the oxidation of CO-like intermediates from methanol dehydrogenation, and enhance the adsorption and oxidation of methanol molecules. Ni shows a worse electrocatalytic performance than that of Pd. However, Ni, which is an oxophilic element like Ru, has the capacity to generate OH_{ads} at a lower potential, and facilitates the oxidative desorption of the intermediate products, thus enhancing both the catalytic activity and stability of Pd catalysts [37,38]. Theoretical analysis has suggested that Pd-Ni alloys may be potentially good catalysts with activity similar to that of Pt-Ru [36]. Besides the alloying effect of Ni, the existence of NiO may also improve the catalytic activity of $Pd_{40}Ni_{60}$ because Shen and Xu [39] have found that metal oxides like NiO have a promoted effect on Pd/C electrocatalysts. Hence, the nanocrystalline PdNi alloy has shown an enhanced electrocatalytic activity towards alcohol oxidation in alkaline solutions, which is a promising catalyst in fuel cell applications.

4. Conclusions

Novel nanocrystalline $Pd_{40}Ni_{60}$ alloy can be fabricated by dealloying a ternary $Al_{75}Pd_{10}Ni_{15}$ precursor in the 20 wt.% NaOH solution under free corrosion conditions. The $Pd_{40}Ni_{60}$ alloy forms a solid solution where both nanocrystalline and amorphous zones can be observed, together with lattice distortion. Compared to NPPd, the nanocrystalline $Pd_{40}Ni_{60}$ alloy has a higher catalytic activity towards electro-oxidation of methanol and ethanol in the alkaline media, a higher stability and a better tolerance to accumulation of carbonaceous species. The nanocrystalline $Pd_{40}Ni_{60}$ alloy fabricated by dealloying is a promising electrocatalyst candidate for direct alcohol fuel cells.

Acknowledgements

The authors acknowledge financial support by National Natural Science Foundation of China (50971079), Independent Innovation Foundation of Shandong University (2010JQ015), and 2nd special support from China Postdoctoral Science Foundation (200902555).

References

[1] C. Bianchini, P.K. Shen, Chem. Rev. 109 (2009) 4183.
[2] K.Y. Chan, J. Ding, J. Ren, S. Cheng, K.Y. Tsang, J. Mater. Chem. 14 (2004) 505.
[3] S.Q. Song, W.J. Zhou, Z.H. Zhou, L.H. Jiang, G.Q. Sun, Q. Xin, V. Leontidis, S. Kontou, P. Tsiakaras, Int. J. Hydrogen Energy 30 (2005) 995.
[4] H.Q. Li, G.Q. Sun, L. Cao, L.H. Jiang, Q. Xin, Electrochim. Acta 52 (2007) 6622.
[5] R. Dillon, S. Srinivasan, A.S. Arico, V. Antonucci, J. Power Sources 127 (2004) 112.
[6] R.N. Singh, A. Singh, Anindita Int. J. Hydrogen Energy 34 (2009) 2052.
[7] M. Baldauf, D.M. Kolb, Electrochim. Acta 38 (1993) 2145.
[8] N. Hoshi, K. Kida, M. Nakamura, M. Nakada, K. Osada, J. Phys. Chem. B 110 (2006) 12480.
[9] V. Radmilovic, H.A. Gasteiger, P.N. Ross, J. Catal. 154 (1995) 98.
[10] K. Wang, H.A. Gasteiger, N. Markovic, P.N. Ross, Electrochim. Acta 41 (1996) 2587.
[11] M.K. Min, J. Cho, K. Cho, H. Kim, Electrochim. Acta 45 (2000) 4211.
[12] Z.L. Liu, X.H. Zhang, L. Hong, Electrochem. Commun. 11 (2009) 925.
[13] C.C. Qiu, R. Shang, Y.F. Xie, Y.R. Bu, C.Y. Li, H.Y. Ma, Mater. Chem. Phys. 120 (2010) 323.
[14] C.Y. Du, M. Chen, W.G. Wang, G.P. Yin, P.F. Shi, Electrochem. Commun. 12 (2010) 843.
[15] X.G. Wang, W.M. Wang, Z. Qi, C.C. Zhao, H. Ji, Z.H. Zhang, Electrochem. Commun. 11 (2009) 1896.
[16] P. Scherrer, N.G.W. Gottingen, Math.-Pys. Kl. 2 (1918) 96.
[17] X.G. Wang, W.M. Wang, Z. Qi, C.C. Zhao, H. Ji, Z.H. Zhang, J. Power Sources 195 (2010) 6740.
[18] Z.H. Zhang, Y. Wang, Z. Qi, J.K. Lin, X.F. Bian, J. Phys. Chem. C 113 (2009) 1308.
[19] X.G. Wang, Z. Qi, C.C. Zhao, W.M. Wang, Z.H. Zhang, J. Phys. Chem. C 113 (2009) 13139.
[20] Z. Qi, C.C. Zhao, X.G. Wang, J.K. Lin, W. Shao, Z.H. Zhang, X.F. Bian, J. Phys. Chem. C 113 (2009) 6694.
[21] Z. Qi, Z.H. Zhang, H.L. Jia, Y.J. Qu, G.D. Liu, X.F. Bian, J. Alloys Compd. 472 (2009) 71.
[22] L. Sun, C.-L. Chien, P.C. Searson, Chem. Mater. 16 (2004) 3125.
[23] M. Hakamada, M. Mabuchi, J. Alloys Compd. 485 (2009) 583.
[24] M.A. Abdel Rahim, R.M. Abdel Hameed, M.W. Khalil, J. Power Sources 134 (2004) 160.
[25] R. Pattabiraman, Appl. Catal. A 153 (1997) 9.
[26] Y.C. Zhao, X.L. Yang, J.N. Tian, F.Y. Wang, L. Zhan, Int. J. Hydrogen Energy 35 (2010) 3249.
[27] C.W. Xu, Y.L. Liu, D.S. Yuan, Int. J. Electrochem. Sci. 2 (2007) 674.
[28] Y.W. Lee, S.B. Han, K.W. Park, Electrochem. Commun. 11 (2009) 1968.
[29] J. Liu, J. Ye, C. Xu, S.P. Jiang, Y. Tong, Electrochem. Commun. 9 (2007) 2334.
[30] M.W. Xu, G.Y. Gao, W.J. Zhou, K.F. Zhang, H.L. Li, J. Power Sources 175 (2008) 217.
[31] J.C. Huang, Z.L. Liu, C.B. He, L.M. Gan, J. Phys. Chem. 109 (2005) 16644.
[32] Q.G. He, W. Chen, S. Mukerjee, S.W. Chen, F. Laufek, J. Power Sources 187 (2009) 298.
[33] M. Sevilla, C. Sanchís, T. Valdés-Solís, E. Morallón, A.B. Fuertes, Electrochim. Acta 54 (2009) 2234.
[34] Z.X. Liang, T.S. Zhao, J.B. Xu, L.D. Zhu, Electrochim. Acta 54 (2009) 2203.
[35] M.V. Martinez-Huerta, S. Rojas, J.L. Gomez de la Fuente, P. Terreros, M.A. Pena, J.L.G. Fierro, Appl. Catal. B: Environ. 69 (2006) 75.
[36] U.B. Demirci, J. Power Sources 173 (2007) 11.
[37] V. Bambagioni, C. Bianchini, J. Filippi, W. Oberhauser, A. Marchionni, F. Vizza, R. Psaro, L. Sordelli, M.L. Foresti, M. Innocenti, ChemSusChem 2 (2009) 99.
[38] S.Y. Shen, T.S. Zhao, J.B. Xu, Y.S. Li, J. Power Sources 195 (2010) 1001.
[39] P.K. Shen, C.W. Xu, Electrochem. Commun. 8 (2006) 184.